Neurobiology of Disease 138 (2020) 104792

Contents lists available at ScienceDirect

Neurobiology of Disease

journal homepage: www.elsevier.com/locate/ynbdi

UsnRNP trafficking is regulated by stress granules and compromised by mutant ALS proteins

Simona Rossi[a,b,*], Valentina Rompietti[a], Ylenia Antonucci[a], Daniela Giovannini[a], Chiara Scopa[c], Silvia Scaricamazza[b], Raffaella Scardigli[a,c], Gianluca Cestra[d,e], Annalucia Serafino[a], Maria Teresa Carrì[b], Nadia D'Ambrosi[b], Mauro Cozzolino[a,*]

[a] Istituto di Farmacologia Traslazionale (IFT), CNR, 00133 Rome, Italy
[b] Dipartimento di Biologia, Università di Roma "Tor Vergata", Rome, Italy
[c] European Brain Research Institute (EBRI), Rome, Italy
[d] Istituto di Biologia e Patologia Molecolari (IBPM), CNR, Rome, Italy
[e] Dipartimento di Biologia e Biotecnologia "Charles Darwin", Università di Roma "Sapienza", Rome, Italy

ARTICLE INFO

Keywords:
ALS
Nucleo-cytoplasmic transport
Integrated stress response
Stress granules
Cajal bodies
Gems

ABSTRACT

Activation of the integrated stress response (ISR), alterations in nucleo-cytoplasmic (N/C) transport and changes in alternative splicing regulation are all common traits of the pathogenesis of Amyotrophic Lateral Sclerosis (ALS). However, whether these processes act independently from each other, or are part of a coordinated mechanism of gene expression regulation that is affected in pathogenic conditions, is still rather undefined. To answer these questions, in this work we set out to characterise the functional connections existing between ISR activation and nucleo-cytosol trafficking and nuclear localization of spliceosomal U-rich small nuclear ribonucleoproteins (UsnRNPs), the core constituents of the spliceosome, and to study how ALS-linked mutant proteins affect this interplay. Activation of the ISR induces a profound reorganization of nuclear Gems and Cajal bodies, the membrane-less particles that assist UsnRNP maturation and storage. This effect requires the cytoplasmic assembly of SGs and is associated to the disturbance of the nuclear import of UsnRNPs by the snurportin-1/importin-β1 system. Notably, these effects are reversed by both inhibiting the ISR or upregulating importin-β1. This indicates that SGs are major determinants of Cajal bodies assembly and that the modulation of N/C trafficking of UsnRNPs might control alternative splicing in response to stress. Importantly, the dismantling of nuclear Gems and Cajal bodies by ALS-linked mutant FUS or C9orf72-derived dipeptide repeat proteins is halted by overexpression of importin-β1, but not by inhibition of the ISR. This suggests that changes in the nuclear localization of the UsnRNP complexes induced by mutant ALS proteins are uncoupled from ISR activation, and that defects in the N/C trafficking of UsnRNPs might play a role in ALS pathogenesis.

1. Introduction

Defects in nucleo-cytoplasmic (N/C) trafficking of proteins and RNAs have emerged as a leading pathogenic mechanism of motor neuron degeneration in Amyotrophic Lateral Sclerosis (ALS) (Kim and Taylor, 2017). Indeed, expanded G4C2 repeats in the C9orf72 gene, which are associated to the most frequent genetic form of ALS, cause transport defects between the nucleus and the cytoplasm (Freibaum et al., 2015; Rossi et al., 2015). Further, mutations in two other ALS-linked genes, TDP43 and FUS, not only directly affect their nucleo-cytosolic distribution, but also have an impact on the overall mechanisms of N/C trafficking (Chou et al., 2018; Dormann et al., 2010; Steyaert et al., 2018). Despite this evidence, how N/C transport alterations are induced in ALS conditions is still poorly defined. It has been recently shown that activation of the integrated stress response (ISR) induces the accumulation into stress granules (SGs) of a number of factors that are central mediators of N/C transport, including import and export factors such as importin-β1, −β2, −α1 and Exportin-1, as well as nucleoporins (Nups), the core subunits of the nuclear pore complex (Woerner et al., 2016; Zhang et al., 2018). As a consequence,

Abbreviations: ISR, Integrated Stress Response; ALS, Amyotrophic Lateral Sclerosis; SGs, Stress Granules; CBs, Cajal Bodies; N/C transport, Nucleo-Cytoplasmic transport

* Corresponding authors at: Istituto di Farmacologia Traslazionale (IFT), CNR, 00133 Rome, Italy.
E-mail addresses: simona.rossi@ift.cnr.it (S. Rossi), mauro.cozzolino@ift.cnr.it (M. Cozzolino).

https://doi.org/10.1016/j.nbd.2020.104792
Received 15 December 2019; Received in revised form 24 January 2020; Accepted 3 February 2020
Available online 04 February 2020

these factors are less available to fulfil their functions, eventually leading to modifications of N/C transport efficiency (Zhang et al., 2018). Thus, a functional connection between the activation of the ISR, SG formation and the regulation of N/C trafficking has been uncovered. Most interestingly, the N/C alterations induced by the expression of mutant ALS genes, which are known to activate the ISR and to induce the assembly of SGs, are somehow reversed by pharmacological inhibition of the ISR, suggesting that in ALS conditions the two events are causally linked (Zhang et al., 2018).

How the activation of the ISR and the resulting regulation of the N/C trafficking affect the nuclear and cytosolic distribution of UsnRNPs, the key constituents of the spliceosome machinery, has not been investigated so far. The biogenesis of UsnRNPs is an intricate process that starts in the nucleus of cells, where the UsnRNAs (U1, U2, U4, U5, U6, U11, U12, U4atac and U6atac) are transcribed by RNA polymerases and modified to become export-competent. Once in the cytosol, UsnRNAs are targeted by the survival of motor neurons (SMN) and protein arginine methyltransferase 5 (PMRT5) complexes, which assist the formation of the Sm core domain. After further modifications, the UsnRNPs, as well as the SMN complex, move back to the nucleus where they undergo final maturation steps, which mostly occur in membraneless nuclear organelles, the Cajal bodies and Gems, respectively (Fischer et al., 2011; Gruss et al., 2017; Matera and Wang, 2014).

The N/C trafficking of UsnRNPs is assisted by complex reactions. The nuclear export of UsnRNAs requires the addition at the 5′ end of a 7 methylguanosine cap (m^7G cap) that is then recognised by the cap-binding complex and exported by CRM1 in a Ran-GTP-dependent manner. The nuclear import of assembled UsnRNPs requires an hypermethylation of the m^7G cap to produce a trimethylguanosine cap (m_3G cap) which is bound by an import adaptor, snurportin-1 (SPN1). SPN1 in turn binds the import receptor importin-β1, eventually promoting the nuclear transfer of UsnRNPs via the nuclear pore complex (Lott and Cingolani, 2011). In this process, the SMN complex is also supposed to have a role (Narayanan et al., 2002).

Indications that some of these events are disturbed in ALS come from circumstantial data showing that ALS-linked mutant proteins induce the cytosolic accumulation of UsnRNAs and associated Sm proteins (Gerbino et al., 2013; Reber et al., 2016; Yin et al., 2017; Yu et al., 2015). Further, this is linked to a decrease in the nuclear distribution of UsnRNPs into Cajal bodies, as well as a decrease in the number of nuclear Gems (Mirra et al., 2017; Nussbacher et al., 2019). However, although it is believed that modifications in the biogenesis and localization of UsnRNPs might underlie the wide splicing defects that characterise motor neuron degeneration in ALS, it is still unknown if the ALS-linked alterations in UsnRNP distribution and splicing regulation and the activation of the ISR, which also occurs in ALS, are pathologically coupled.

To answer these questions, in this work we have characterised the functional connections between ISR activation, SG formation and the N/C trafficking of spliceosomal UsnRNPs, and studied how ALS-associated proteins, such as mutant FUS and C9orf72-derived dipeptide repeat proteins (C9-DPRs), affect this interplay.

2. Material and methods

2.1. Antibodies and reagents

The following primary antibodies were used: rabbit anti-ATF4 (Santa Cruz Biotechnology); rabbit anti-Phospho-eIF2α (Ser51) (D9G8) (Cell Signaling technology); rabbit anti-eIF2α (D7D3) (Cell Signaling technology); rabbit anti-Lamin B1 (Abcam); rabbit anti-snurportin-1 (Proteintech); mouse anti-KPNB1 (3E9) (Abcam); rabbit GAPDH (FL-335) (Santa Cruz Biotechnology); mouse GFP (Abcam); mouse anti-β-actin (SIGMA); mouse anti-c-MYC (9E10) (SIGMA); mouse anti-FLAG M2 (SIGMA); rabbit anti-FLAG (SIGMA); mouse anti-Puromycin (12D10) (Millipore); goat anti-TIA-1 (Santa Cruz Biotechnology); mouse anti-TIAR (BD Transduction Laboratories); rabbit anti-Coilin (Proteintech); goat anti-Cholin Acetyltransferase (ChAT) (Merck Millipore); mouse anti-SMN (SIGMA) for immunofluorescence analysis, mouse anti-SMN (BD Transduction Laboratories) for western blot detection; rabbit anti-Gemin2 (Proteintech); mouse anti-Sm B/B′ (Thermo Scientific). Anti-rabbit, anti-mouse and anti-goat IgG peroxidase-conjugated secondary antibodies were from Bio Rad; Alexa-Fluor-488 and Cy3-conjugated secondary antibodies were from Jackson ImmunoResearch Laboratories; Alexa-Fluor-647 secondary antibodies were from Invitrogen. Sodium arsenite, thapsigargin, ISRIB, puromycin and cyclohexymide were from SIGMA. PERK inhibitor GSK2606414 was from Calbiochem. Dextrane sulfate was from Millipore, *E. coli* tRNA from Roche, and single-stranded (ss)DNA from SIGMA. All other reagents were from SIGMA.

2.2. DNA synthesis and plasmid construction

pEGFP-N1 coding importin-β1 was a kind gift of Dr. Patrizia Lavia. pCMV plasmids coding 100 dipeptides Glycine-Arginine (GR), Proline-Arginine (PR) or Glycine-Alanine (GA), fused with a N-terminal FLAG tag, were kindly provided by Prof. Angelo Poletti (Cristofani et al., 2018). Wild type (WT) and mutant (P525L) human FUS were PCR-amplified from human cDNA and cloned in fusion with a N-terminal 3xFLAG tag in pcDNA3.1 plasmid (Invitrogen). Wild type human eIF2α were PCR-amplified from human cDNA and cloned in fusion with a C-terminal 6xMYC tag in pCS2 + MT plasmid. WT eIF2α was then mutagenized by PCR-driven overlap extension to generate S51A eIF2α, and cloned into pCS2 + MT-6xMYC plasmid. All sequences were verified by automated DNA sequencing.

2.3. Cell culture, treatments and transfection

HeLa cells were grown in Dulbecco's modified Eagle's medium (DMEM) with Glutamax (Corning) supplemented with 10% fetal bovine serum (FBS, Euroclone) at 37 °C in an atmosphere of 5% CO_2 in air. To induce the integrated stress response, cells were maintained in culture for 24 h prior to treatments with sodium arsenite (NaAs) or thapsigargin (TG) at the indicated doses and times. In general, cells were treated with 0.3 mM NaAs for 1 h to analyse eIF2α phosphorylation, for 4 h to evaluate SG formation and to count Cajal and Gems bodies, and for 6 h to analyse alternative splicing changes. Where specified, cells were pre-treated with 10 μg/ml ISRIB for 4 h. Otherwise, cells were treated with 40 μM TG for 1 h, and, where specified, were pre-treated with 100 μM GSK2606414 for 2 h. For transient expression of mutant ALS proteins, cells at 80% confluence were transfected using Lipofectamine 2000 (Invitrogen), according to the manufacturer's instruction, and collected after 24 h. Where specified, cells were treated with 10 μg/ml ISRIB or 20 μM GSK2606414 just following transfection. D7-E2_GFP motor neuron (MN) progenitors were derived from embryonic spinal cord of transgenic E2-GFP transgenic mice (Medelin et al., 2018; Scardigli et al., 2001). Briefly, cells were isolated from spinal cord tissue by enzymatic digestion (1.33 mg/ml trypsin, 0.7 mg/ml hyaluronidase, and 0.2 mg/ml kynurenic acid) (SigmaAldrich) for 30 min at 37 °C and mechanical dissociation with small-bore Pasteur pipette. Cells were plated at 10^4 cells/cm^2 cells density and cultured as neurospheres in growth medium, as described (Scardigli et al., 2014). Growth factors were replenished weekly. To assess for differentiation, neurospheres were dissociated into single cells and plated onto matrigel-coated glass coverslips (12 mm diameter) at 5×10^4 cells/cm^2 in differentiating medium (growth medium without EGF and FGF and supplemented with 10 ng/ml BDNF, 10 ng/ml NT-3 and 10 ng/ml GDNF, Peprotech). Half medium was replaced every other day. Two weeks after plating, differentiated cells were fixed in 4% PFA at RT for 10 min and processed for immunocytochemistry.

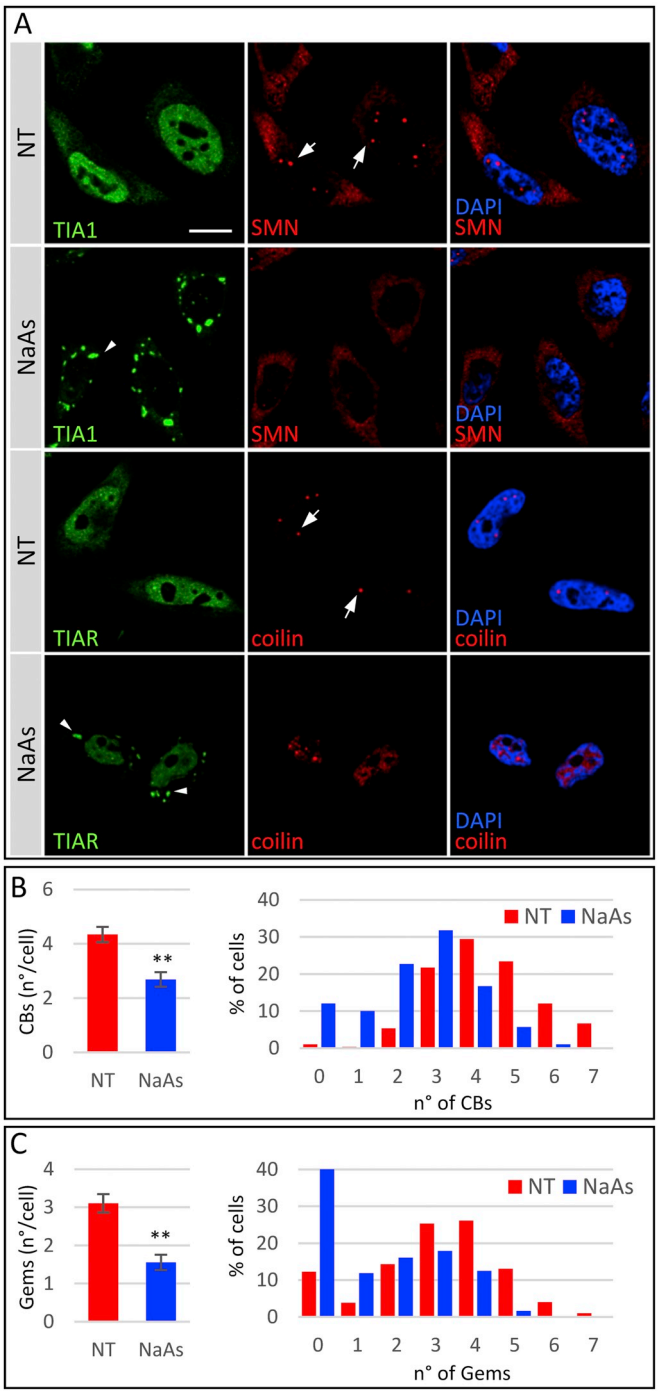

Fig. 1. ISR activation induces the decrease of nuclear Gems and Cajal bodies. HeLa cells were left untreated (NT) or treated with 0.3 mM NaAs for 4 h (NaAs), and stained with anti-TIAR or TIA1 antibodies to detect stress granules (green), anti-SMN, a specific marker of Gems (red), and anti-coilin, a specific Cajal body (CB) protein (red). Nuclei were detected by DAPI staining (blue). (A) Representative images are presented. Coilin-positive nuclear CBs and SMN-positive nuclear Gems are indicated by arrows. Arrowheads point to cytosolic stress granules. Scale bar: 10 μm. Nuclear CBs (B) and Gems (C) were counted in each condition. The number of CBs (B) and Gems (C) that are present in the nuclei of untreated (NT) or treated (NaAs) cells were scored and reported as mean ± SD (left panels). The distribution of cells (%) classified according to the number of SMN- and Coilin-positive granules per nucleus is also reported. At least 100 cells per condition in $n \geq 5$ independent experiments have been scored. $^{**}P < .01$ by *t*-test versus NT cells is shown. (For interpretation of the references to colour in this figure legend, the reader is referred to the web version of this article.)

2.4. Immunofluorescence and FISH analysis

Cell cultures, seeded on poly-L-lysine-coated glass coverslips, were washed in PBS and fixed with 4% paraformaldehyde in PBS for 10 min. After washing in PBS, cells were permeabilized with 0.1% Triton X-100 in PBS for 5 min, and then blocked for 30 min in PBS containing 2% FBS. Incubation with primary antibodies, properly diluted in PBS, 2% FBS, was carried out for 1 h at 37 °C in a humidified chamber. After three washes in PBS, cells were then incubated with fluorophore-conjugated secondary antibodies diluted in PBS, 2% FBS for 45 min at room temperature. After rinsing in PBS, cells were stained with 1 μg/ml DAPI in PBS for 5 min. Differentiated primary motor neurons were processed as described (Medelin et al., 2018). Fluorescence in situ hybridization (FISH) analysis was performed as previously described, except that 30% formamide was used in all steps (Rossi et al., 2015). Sense (S) and antisense (AS) U2 RNA probes were generated as previously described (Gerbino et al., 2013). Cells were analysed with a LEICA TCS SP5 confocal microscope and processed using LAS AF and Adobe Photoshop software.

2.5. Protein extraction and nuclear-cytosolic fractionation

After rinsing with ice-cold PBS, cells were lysed on ice for 10 min in RIPA buffer (50 mM Tris-HCl, pH 7.4, 1% Triton X-100, 0.25% Na-deoxycholate, 0.1% SDS, 150 mM NaCl, 1 mM EDTA, 5 mM $MgCl_2$, protease inhibitor cocktail), and then centrifuged at 17,000*g* for 5 min. Supernatants containing total protein extracts were quantified using Bradford protein assay (Bio-Rad) and resuspended in Laemmli Buffer for SDS-PAGE. For translation rate analysis, prior of cell lysis, cell cultures were treated with 10 μg/ml puromycin for 10 min at 37 °C. Where specified, cells were previously treated with 10 μM cycloheximide for 10 min at 37 °C. For the isolation of nuclear and cytoplasmic proteins, cells were centrifuged at 600*g* at 4 °C for 5 min. Cell pellets were resuspended by gentle pipetting with ice-cold hypotonic lysis buffer (HLB) containing 10 mM Tris, pH 7.5, 10 mM NaCl, 3 mM $MgCl_2$, 0.1% NP-40, 10% glycerol and protease inhibitor cocktail, and incubated on ice for 10 min. A fraction of lysates was transferred in a new tube supplemented with Laemmli buffer to obtain total protein extract, while the remaining lysates were centrifuged at 1000*g* at 4 °C for 3 min. Supernatants containing cytoplasmic fraction were clarified with an additional centrifugation at 5000*g* for 5 min, while nuclei pellets were washed three times by gently pipetting with ice-cold HLB and centrifuging at 300*g* at 4 °C for 2 min. To obtain total nuclear extracts, pellets were resuspended in Laemmli buffer. Electrophoresis and Western blot were performed as described (Rossi et al., 2015). Membranes were developed using Clarity™ Western ECL substrate (Bio Rad). Densitometric analyses were performed using ImageJ software program (National Institutes of Health).

2.6. Filter retardation assay

After rinsing with ice-cold PBS, C9-DPR-transfected cells were lysed in PBS supplemented with a cocktail of protease inhibitors by freeze-thaw for three times. Total protein extracts were then centrifuged at 16000*g* at 4 °C for 5 min, and supernatants were quantified using Bradford protein assay (Bio-Rad). Equal amounts of total proteins were filtered through a 0.2 μm cellulose acetate membrane (Whatman) using a Bio-Dot Microfiltration Apparatus (Bio-Rad). The membranes were then analysed by Western blot.

2.7. RNA methods

Total RNAs were extracted using TRIzol (Invitrogen) and treated with RNAse-free DNase (Promega), according to the manufacturer's instruction. 1 μg of RNA and random primers were used to generate first-strand cDNA by Im-Prom II reverse transcription system

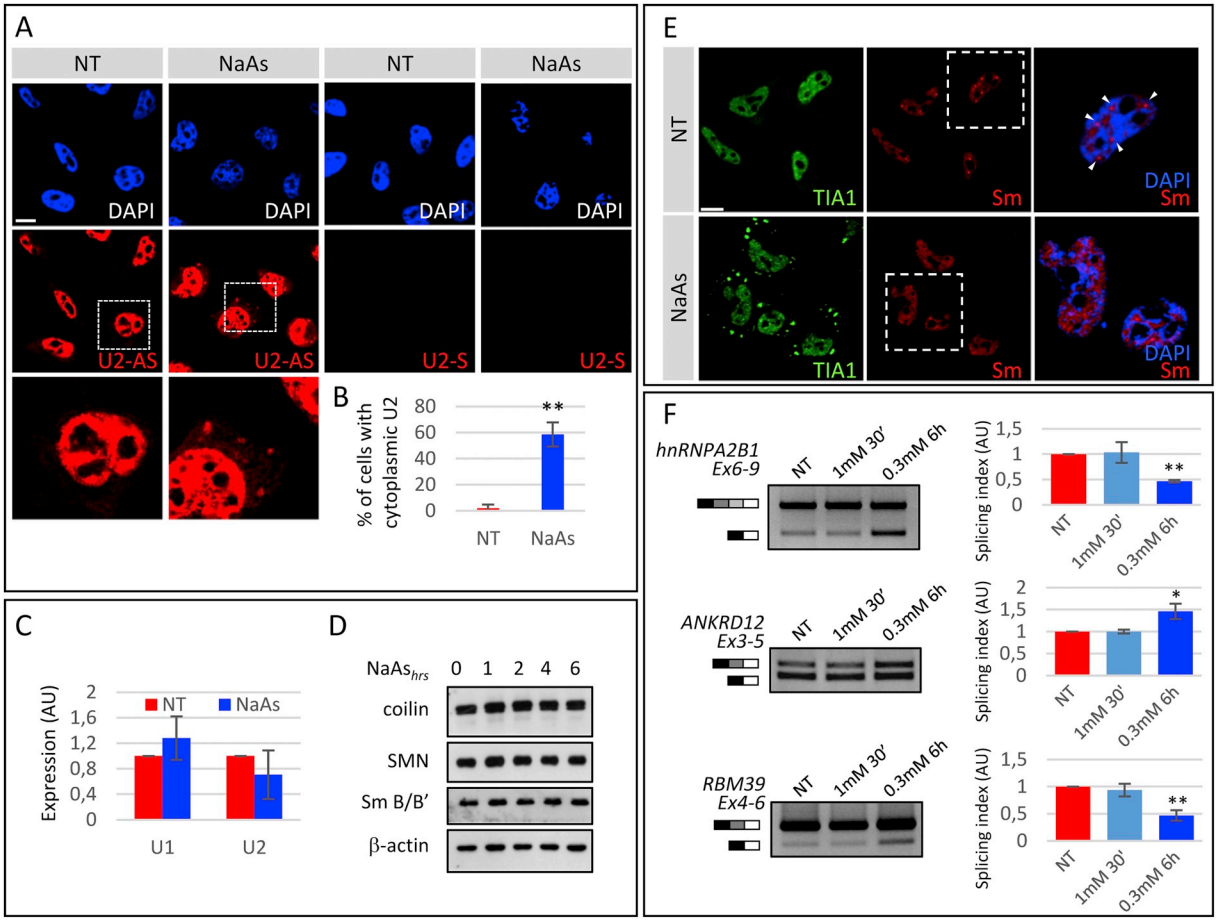

Fig. 2. ISR activation induces delocalization of UsnRNPs and changes in alternative splicing. HeLa cells were left untreated (NT) or treated with 0.3 mM NaAs for 4 h (NaAs). (A) Shown is the in-situ hybridisation with a probe recognising the U2snRNA (U2-AS, red). A control probe (U2-S) was also used as control for the specificity of the reaction. Nuclei were stained with DAPI (blue). Magnifications are shown to highlight the presence of U2-positive cytosolic granules in NaAs treated cells. Scale bar: 10 μm. (B) The percentage of cells with cytoplasmic staining of U2snRNA was scored ($n = 3$ independent experiments, $^{**}P < .01$ by t-test versus NT cells). (C) RT-qPCR to quantify the levels of the indicated UsnRNAs in NT or NaAs-treated cells. Shown are the levels (AU) of expression normalised to the housekeeping BC200 and GAPDH RNAs. Mean ± SD is shown (n = 3). (D) Expression levels of coilin, SMN, Sm B/B′ and β-actin were assayed by Western blot on cells untreated or treated with 0.3 mM NaAs for the indicated time. The panel is representative of $n = 3$ independent experiments. (E) HeLa cells were left untreated (NT) or treated with 0.3 mM NaAs for 4 h (NaAs). An Y12 antibody recognising the Sm core of assembled UsnRNPs was used in immunofluorescence analysis to monitor the nuclear localization of UsnRNPs (red). TIA1 was stained with a specific antibody to monitor stress granule formation (green). Nuclei are shown in blue (DAPI). Merged representative magnifications of the highlighted areas are also shown. Arrowheads point to nuclear UsnRNPs. Scale bar: 10 μm. (F) HeLa cells were left untreated (NT) or treated with 1 mM or 0.3 mM NaAs for 30 min or 6 h, respectively. The presence or absence of the indicated exons in the hnRNP A2/B1, ANKRD12 and RBM39 genes were assayed by PCR as a measure of alternative splicing changes. Bands from the experiments were quantified by densitometry analysis, and a splicing index was calculated as the ratio between the upper and the lower bands and scaled to have the average ratio in NT cells as 1. The mean ± SD from $n = 3$ independent experiments is reported. $^{*}P < .05$ by *t*-test versus NT cells is shown. (For interpretation of the references to colour in this figure legend, the reader is referred to the web version of this article.)

(Promega), according to the manufacturer's instruction. Quantitative real-time PCR (qPCR) was performed with iTaq Universal SYBR Green Supermix (Bio-Rad) using 0.5 ng cDNA and 350 nM of specific primers, listed in Supplemental Table S1. qPCR reactions were performed using the CFX Connect Real-Time PCR Detection System (Bio-Rad). Cq values were determined from the system software using 'single threshold' mode. The relative expression level of UsnRNAs were calculated from these Cqs using experimentally determined amplification efficiencies, and then normalised for the housekeeping genes GAPDH and BC200. For the detection of the different isoforms of hnRNP A2/B1, ANKRD12 and RBM39, PCR reactions were performed with Biomix Red (Bioline) using 50 ng cDNA and specific primers listed in Supplemental Table S1. To ensure quantitative measurements during the linear phase, the number of cycles was experimentally determined. PCR products were resolved in 2% agarose gels and visualized by ethidium bromide staining. Images were acquired on a Geldoc imaging system (Biorad), and the splicing indices were calculated as the ratio between the upper and the lower bands after densitometric analysis using the ImageJ software (National Institute of Health).

2.8. Statistical analysis

Statistical analysis was performed with unpaired two-tailed Student's *t*-test for comparison between two groups, otherwise with one-way ANOVA followed by Tukey's test, using GraphPad Prism 6 software. Values significantly different from the relative control are indicated with asterisks. *P*-values ≤.05 or ≤.01 were considered significant.

3. Results

3.1. ISR activation causes the dismantling of nuclear Gems and Cajal bodies

The activation of the ISR induces the recruitment into stress

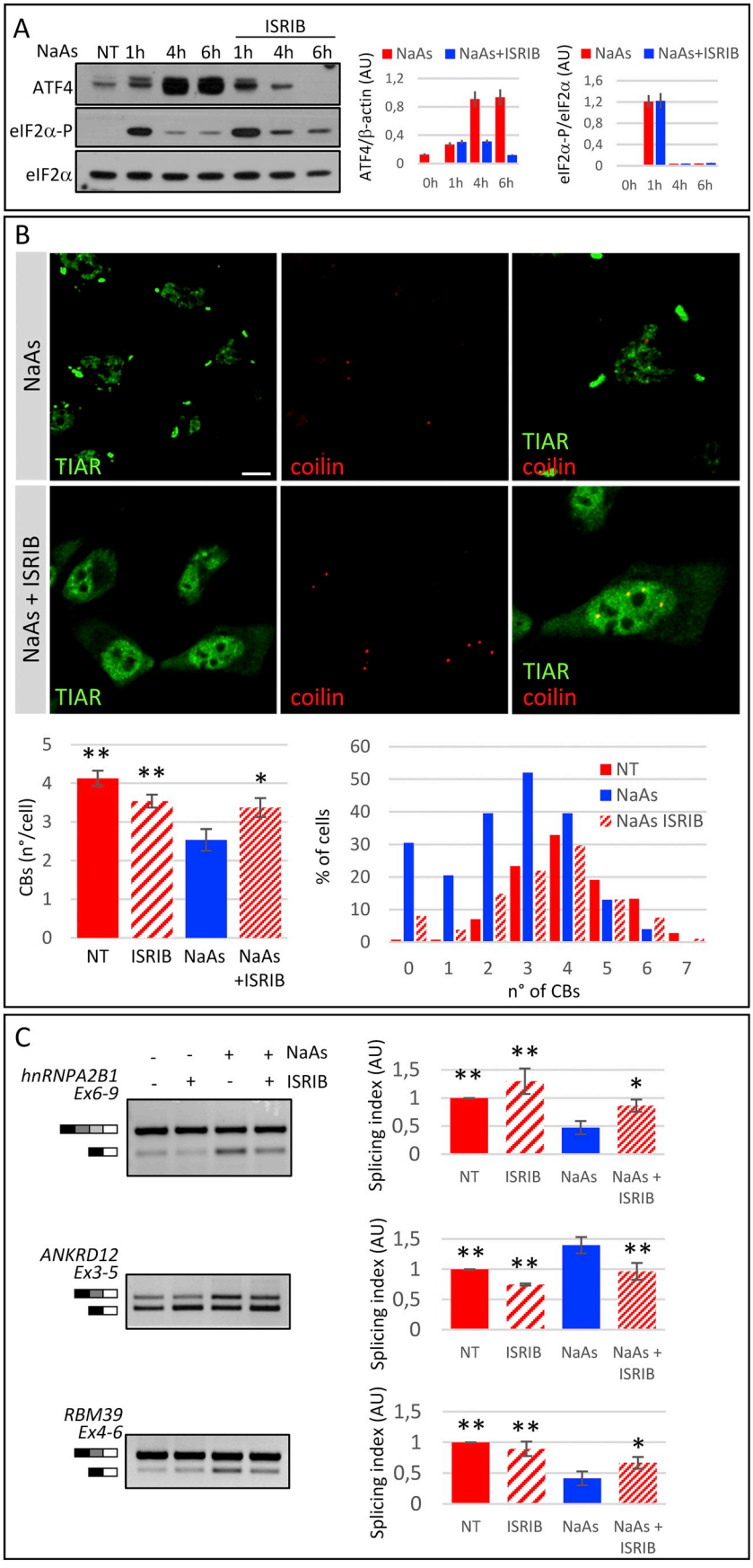

Fig. 3. UsnRNP mislocalization is reversed by ISRIB. (A) HeLa cells were treated with 0.3 mM NaAs for the indicated periods in the presence or absence of 10 μg/ml ISRIB, and then analysed by Western blot with antibodies anti-phosphorylated (eIF2α-P) and total eIF2α, and anti-ATF4. A quantification of the experiment shown is displayed in the right panels. (B) Cells treated as in (A) for 4 h were stained with anti-TIAR (green) and anti-coilin (red) antibodies. Scale bar: 10 μm. The number of CBs that are present in untreated (NT) or treated (NaAs) cells, either in the presence or absence of ISRIB, were scored and reported as mean ± SD (left panel). The distribution of cells (%) classified according to the number of CBs is also reported (right panel). At least 100 cells per condition in $n \geq 3$ independent experiments have been scored. $^{**}P < .01$ and $^{*}P < .05$ by one-way ANOVA versus NaAs are shown. (C) The indicated alternative splicing events were assayed by PCR in cells treated with 0.3 mM NaAs for 6 h, either in the presence or absence of ISRIB. A splicing index was calculated as indicated in Fig. 3 and reported on right panels. The experiment shown is representative of n = 3 independent experiments. $^{**}P < .01$ and $^{*}P < .05$ by one-way ANOVA versus NaAs are shown. (For interpretation of the references to colour in this figure legend, the reader is referred to the web version of this article.)

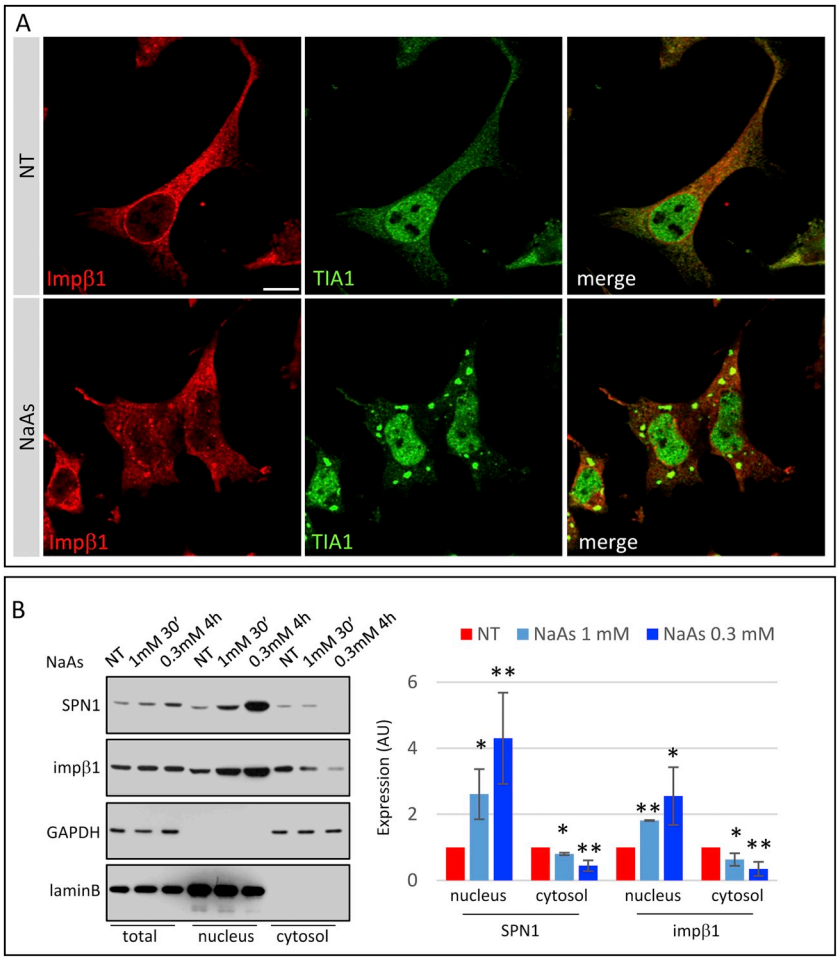

Fig. 4. Activation of the ISR affects the localization of importin-β1 and snurportin-1. (A) HeLa cells were left untreated (NT) or treated with 1 mM NaAs for 30 min, and stained with an anti-TIA1 antibody (green), to detect stress granules, and an anti-importin-β1 antibody (red). Scale bar: 10 μm. (B) Total, nuclear and cytosolic extracts (in a volume ratio of 1:5:1), from cells treated as indicated, were assayed in Western blot for the expression of importin-β1 and SPN1. GAPDH and laminB were also measured to check for the purity of fractions. The nuclear and cytosolic expression levels of SPN1 and importin-β1 were normalised to the expression of laminB and GAPDH, respectively, and the relative ratios were scaled to those of NT cells considered as 1. Means ± SDs from $n = 3$ independent experiments are reported. $^{**}P < .01$ and $^{*}P < .05$ by *t*-test versus NT cells. (For interpretation of the references to colour in this figure legend, the reader is referred to the web version of this article.)

granules of key mediators of nucleo-cytosol communication, eventually leading to alterations of the transport between the two compartments (Zhang et al., 2018). To assess whether these effects might impact on the trafficking and nuclear distribution of UsnRNPs, we first checked the behaviour, under stress conditions, of Gems and Cajal Bodies (CBs). To this aim, HeLa cells were left untreated or were treated with sodium arsenite (NaAs), a well-known inducer of the ISR, and then were analysed by immunofluorescence with antibodies to SMN, that specifically stains nuclear Gems, or to coilin, a specific CB marker. Antibodies anti-TIA1 or TIAR, two specific SG markers, were also used. As shown in Fig. 1, a strong decrease in the average number of Gems and CBs is recorded in cells carrying NaAs-induced SGs. Further, the distribution of cells (%) classified according to the number of SMN- and Coilin-positive granules per nucleus is profoundly affected by NaAs, with stressed cells showing a significant shift of the distribution toward lower number of Gems and CBs. A similar result was obtained in cells treated with thapsigargin (TG), a known inducer of the ISR and SG formation via the activation of PERK-dependent eIF2α phosphorylation, as well as in post-mitotic mouse motor neurons treated with NaAs (Supplemental Fig. S1, S3). Thus, nuclear CBs and Gems undergo a generalized re-organization in response to ISR activation. To assess whether the decrease in the number of these nuclear bodies might be linked to alterations in the nucleo-cytosolic localization of UsnRNPs, FISH analysis using a probe targeting U2snRNA, a major UsnRNP UsnRNAs, was performed in HeLa cells. As illustrated in Fig. 2A,B, the probe for U2 specifically recognises the U2-snRNA in the nucleus of untreated cells. Upon NaAs treatment, a significant proportion of cells displays a cytoplasmic signal of U2snRNA, that clearly accumulates into cytosolic granules. No labelling is observed in the same conditions using a sense probe to U2, which indicates the specificity of the signal obtained. To exclude that this effect might be associated to alterations in the biosynthesis of UsnRNAs, qPCR analysis for U1 and U2snRNAs was performed. As shown in Fig. 2C, no significant differences in the steady state expression of snRNAs are detected. Similarly, no significant differences are observed by Western blot in the expression levels of SMN and coilin, nor in the expression of Sm proteins, the core constituents of UsnRNPs (Fig. 2D). On the contrary, immunofluorescence staining of the Sm-core of UsnRNPs clearly shows a dramatic decrease of nuclear UsnRNP-containing granules (Fig. 2E), in keeping with the observed reduction in CB number. A change in the proper localization of UsnRNPs could cause modifications in alternative splicing patterns. To test this possibility, we analysed the splicing pattern of a set of target genes, that were selected based on their known ability to undergo alternative splicing regulation in response to defects in UsnRNP activity (Mirra et al., 2017; Yin et al., 2017). As shown in Fig. 2F, NaAs induces the skipping of exon 8 from hnRNP A2/B1 mRNA. Similarly, the splicing pattern of ANKRD12 and RBM39 is significantly affected under the same conditions. Thus, the activation of the ISR affects the proper nuclear localization of the SMN complex and UsnRNPs, and induces changes in alternative splicing regulation.

3.2. *Inhibition of stress granules restores Cajal bodies assembly and alternative splicing*

To establish a functional link between the observed changes in alternative splicing regulation and the activation of the ISR, we took advantage of ISRIB, which potently inhibits ISR activation and SG formation acting downstream of eIF2α phosphorylation (Rabouw et al.,

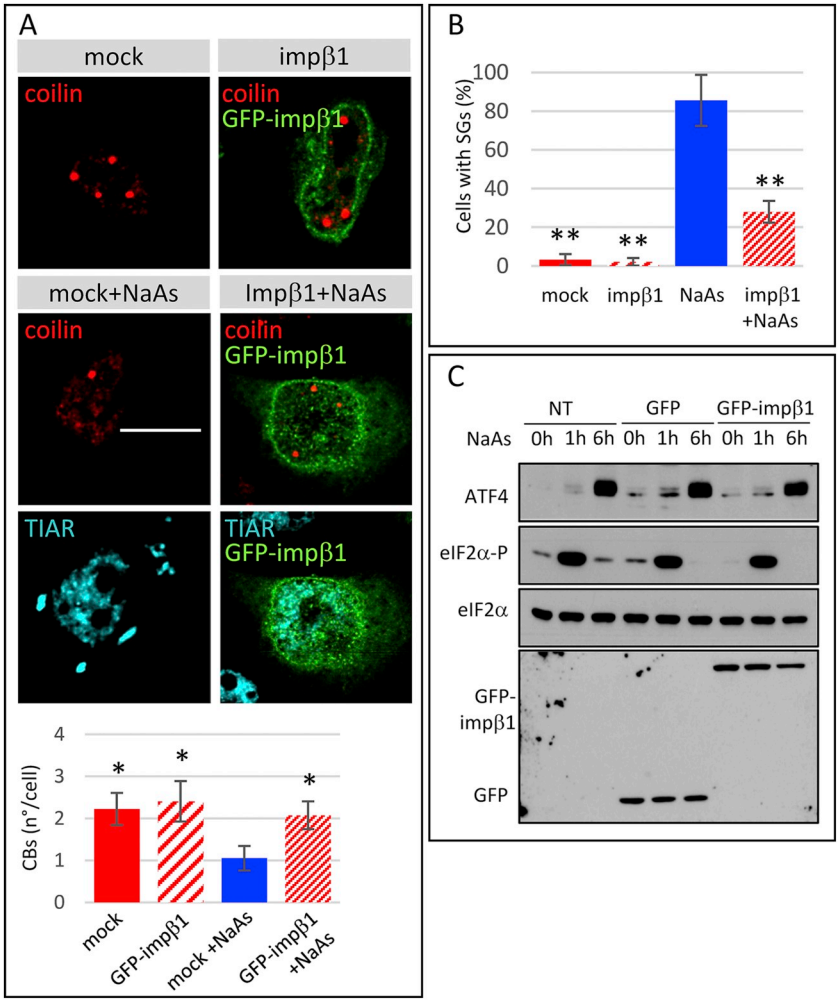

Fig. 5. Expression of importin-β1 restores UsnRNP nuclear localization in stressed cells. (A) HeLa cells were transfected with a mock plasmid or with a plasmid for the expression of GFP-tagged importin-β1. After 24 h, cells were left untreated or were treated with 0.3 mM NaAs for 4 h, and the staining of GFP, TIAR (blue) and coilin (red) was collected by immunofluorescence analysis. Representative merge images are shown. Scale bar: 10 μm. The number of CBs in each condition was scored and is presented as mean ± SD from $n = 3$ independent experiments. $^{*}P < .05$ by one-way ANOVA versus NaAs are shown. (B) The number of stress granules in cells treated as in (A) are presented as mean ± SD from n = 3 independent experiments. $^{**}P < .01$ by one-way ANOVA versus NaAs are shown. (C) HeLa cells were left untrasfected (NT) or transfected with plasmids coding for GFP or GFP-importin-β1, and after 24 h were treated with 0.3 mM NaAs for the indicated periods. Total protein extracts were then subjected to Western blot analysis with antibodies anti-phosphorylated (eIF2α-P) and total eIF2α, anti-ATF4 and anti-GFP. (For interpretation of the references to colour in this figure legend, the reader is referred to the web version of this article.)

2019; Sidrauski, 2015). HeLa cells were treated with NaAs in the presence or absence of 10 μg/ml ISRIB, and the localization of Gems, CBs and SGs was assessed using specific markers. As expected, pre-treatment of cells with ISRIB substantially abolishes ISR activation by NaAs, as measured by its ability to inhibit the upregulation of ATF4 and the formation of SGs, without affecting the phosphorylation of eIF2α (Fig. 3A,B). Most importantly, these effects are associated to an almost complete rescue to control values of the number of CBs and Gems in NaAs-treated cells (Fig. 3B and Supplemental Fig. S2), with the retrieve of their original subcellular localization. Consistently, expression of a dominant-negative, non-phosphorylatable mutant form of eIF2α, which overcomes the translational initiation block, prevents the drop in CB number induced by NaAs (Supplemental Fig. S3). Similarly, the decrease of Cajal and Gem bodies due to thapsigargin treatment is reversed by GSK2606414, a known inhibitor of eIF2α phosphorylation (Supplemental Fig. S3). Finally, a significant recovery in the alternative splicing patterns of hnRNP A2/B1, ANKRD12 and RBM39 is observed in conditions of ISR inhibition (Fig. 3C). Overall, these results indicate that disassembly of CBs, mislocalization of UsnRNPs and alternative splicing changes are a direct consequence of ISR activation. To establish if the formation of SGs is required for this process, we made use of cycloheximide (CHX), a global translation inhibitor that stabilizes polysomes on mRNAs, thus preventing their translocation into SGs and eventually blocking SG formation. Treatment of cells with CHX, which is sufficient to block protein translation, has no effect on nuclear CBs, while it completely prevents SG formation as well as CB disassembly induced by NaAs (Supplemental Fig. S4), indicating that the assembly of cytoplasmic SGs is a major determinant of the observed reduction of CBs upon ISR activation.

3.3. *Defective nuclear localization of UsnRNPs depends upon stress-induced changes of SPN1/importin-β1 localization*

Previous results prompted us to test if the modified nuclear localization of UsnRNPs upon induction of the ISR is a direct consequence of a decreased availability of importin-β1, one of the major player in the nuclear import of UsnRNPs, which has been recently shown to localize into stress granules upon stress (Zhang et al., 2018). To verify this hypothesis, HeLa cells treated with NaAs were stained with an antibody anti-importin-β1. As shown in Fig. 4A, importin-β1 is evenly distributed on the nuclear membrane in untreated cells. In response to NaAs, however, importin-β1 strongly re-localizes into cytosolic TIA1-positive SGs, as well as into perinuclear clusters adjacent to the nuclear envelope. Moreover, a significant accumulation of importin-β1 into nuclear fractions of NaAs-treated cells is recorded, with a concurrent decrease in cytosolic levels (Fig. 4B). Similarly, snurportin-1 (SPN1), the import adaptor for the nuclear import of UsnRNPs, undergoes a strong nuclear accumulation under stress (Fig. 4B). Thus, these results show that the activation of the ISR is associated to a strong rearrangement of two major factors involved in UsnRNP nuclear import, and suggest that defective UsnRNP nuclear localization might be a direct consequence of this effect. To test this possibility, importin-β1 was transiently overexpressed in HeLa cells treated with NaAs. Coilin staining of cells clearly shows that in the presence of an overexpressed importin-β1 the number of CBs in NaAs-treated cells is significantly recovered to control levels (Fig. 5A). Interestingly, the overexpression of importin-β1 has

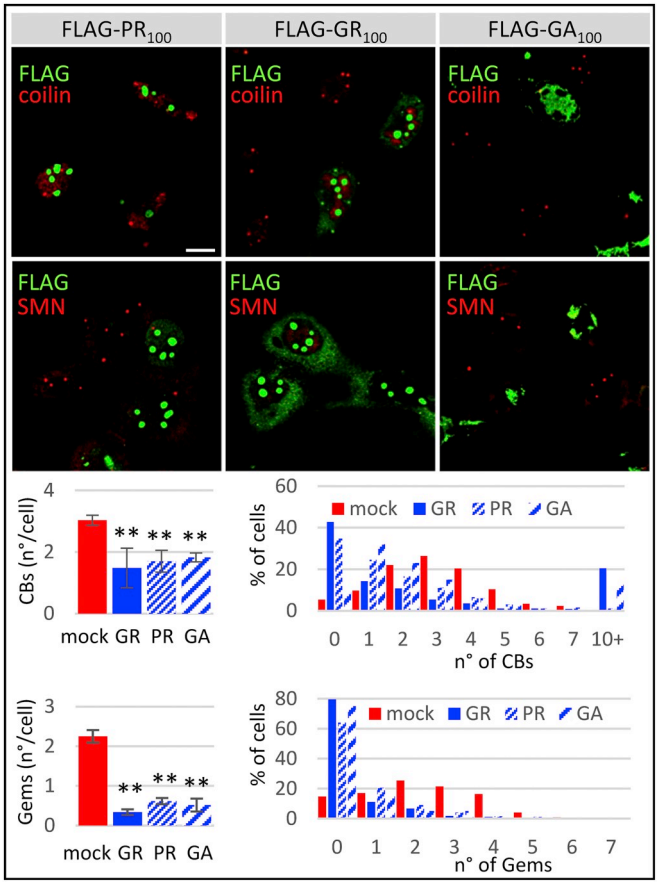

Fig. 6. Expression of C9-DPRs affect nuclear Gems and CBs. The FLAG-tagged C9-DPRs poly-PR, −GR and -GA were overexpressed in HeLa cells by transient transfection, and monitored by immunofluorescence analysis with an anti-FLAG antibody. Coilin and SMN were also co-stained to detect nuclear Gems and Cajal bodies. Merged representative images are shown. Scale bar: 10 μm. The number of CBs and Gems that are present in the nuclei of mock-transfected or DPR-transfected cells was scored and reported as mean ± SD (left panels). The distribution of cells (%) classified according to the number of SMN- and Coilin-positive granules per nucleus is also reported. At least 100 cells per condition in $n \geq 3$ independent experiments have been scored. $^{**}P < .01$ by *t*-test versus mock-transfected cells.

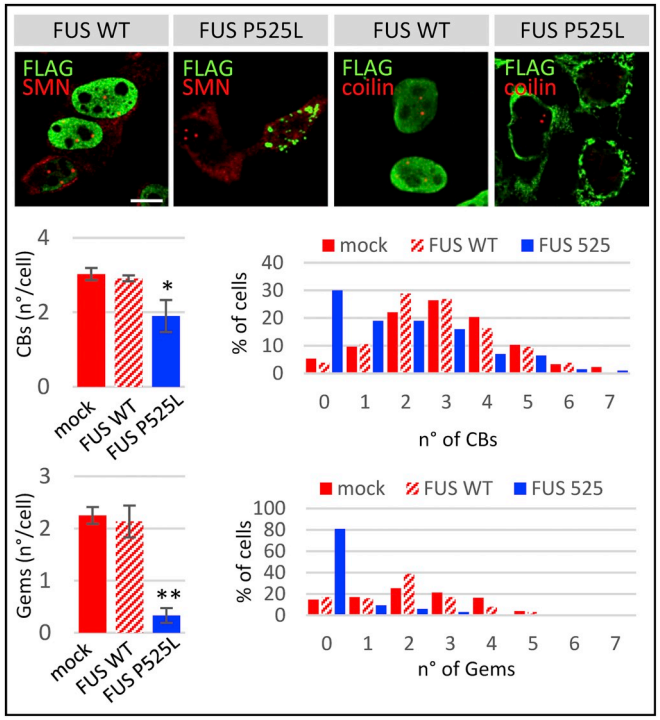

Fig. 7. ALS-linked mutant FUS affects nuclear Gems and CBs. The FLAG-tagged human wild-type (WT) FUS, or the ALS-linked P525L mutant were over-expressed in HeLa cells by transient transfection and monitored by immuno-fluorescence analysis. An anti-FLAG antibody was used to detect transfected FUS. SMN and Coilin were also co-stained to detect nuclear Gems and Cajal bodies. Scale bar: 10 μm. The number of CBs and Gems that are present in the nuclei of mock-transfected or FUS-transfected cells was scored and reported as mean ± SD (left panels). The distribution of cells (%) classified according to the number of SMN- and Coilin-positive granules per nucleus is also reported. At least 100 cells per condition in n ≥ 3 independent experiments have been scored. $^{**}P < .01$ and $^{*}P < .05$ by t-test versus mock-transfected cells.

also a striking effect on SGs, which are significantly decreased in number (Fig. 5B). To exclude that the importin-β1-mediated rescue of UsnRNP trafficking might be caused by the inhibition of the ISR, the level of eIF2α phosphorylation was therefore analysed in cells expressing importin-β1. As shown in Fig. 5C, importin-β1 overexpression does not affect eIF2α phosphorylation and ATF4 upregulation induced by NaAs, indicating that the alteration of UsnRNP nuclear localization and the modification of alternative splicing activity might result from the impairment of importin-β1 function downstream of ISR activation.

3.4. ALS proteins mutFUS and C9-DPRs cause ISR-independent changes in UsnRNP localization

Activation of the ISR, formation of SGs, alteration in N/C transport and changes in alternative splicing regulation are all common traits of ALS pathogenesis. Based on previous results, we therefore asked if a functional connection might exist between these traits. To answer this question, HeLa cells were transiently transfected for the expression of the C9orf72-associated dipeptides (C9-DPRs). Among the five C9-DPRs, poly-GR, -PR and -GA have been repeatedly described to cause toxicity in a number of ALS model systems (Freibaum and Taylor, 2017), and for these reasons were chosen for the following experiments. Further, wild-type and the ALS-linked P525L mutant form of FUS (mutFUS) were also analysed. The expression of DPRs induces the formation of cytosolic stress granules, that occasionally co-localize with cytosolic DPR aggregates that form in a fraction of transfected cells (Supplemental Fig. S5). Similarly, the expression of mutFUS leads to the formation of cytosolic SGs that largely overlap with cytosolic-aggregated mutFUS (Di Salvio et al., 2015). In all these conditions, phosphorylation of eIF2α is increased and global translation is inhibited (Supplemental Fig. S5, and (Di Salvio et al., 2015)). Importantly, these effects are associated to a strong decrease in the number of nuclear Gems and CBs (Figs. 6,7). Notably, in the case of poly-GR and, to a lesser extent, poly-GA, a significant fraction of cells displays an increased number of CBs with reduced size compared to mock-transfected cells (Fig. 6), suggesting that in these conditions the overall dynamics of CB formation might be also affected. To analyse if the observed changes in nuclear localization of CBs might be a result of ISR activation by mutant ALS proteins, transfected cells were treated with ISRIB, which was already shown to inhibit ALS-linked SG formation (Zhang et al., 2018). Surprisingly, the dismantling of nuclear Gems/CBs by mutant ALS proteins is completely unaffected by ISRIB (Fig. 8A,B). Further, GSK2606414, a selective inhibitor of PERK kinase (Fig. 8C) that halts ISR activation upstream of eIF2α phosphorylation, is unable to restore the correct trafficking of UsnRNPs. Similarly, co-expression of non-phosphorylatable form of eIF2α S51A has no significant effects on the decrease of CBs due to C9-DPRs and mutFUS (Fig. 8D). Overall, these results

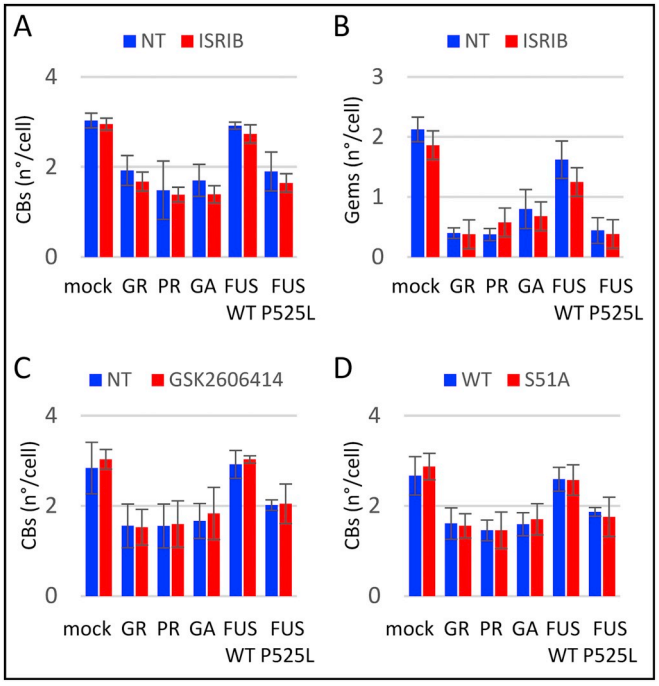

Fig. 8. Inhibition of the ISR does not recover UsnRNP mis-localization induced by mutant ALS proteins. FLAG-tagged mutant ALS proteins were expressed in HeLa cells in the presence or absence of 10 μg/ml ISRIB. After 24 h, CBs (A) and Gems (B) were stained by immunofluorescence analysis and scored in $n = 3$ independent experiments. Means ± SDs are shown. (C) Cells were transfected as in (A) in the presence or absence of 20 μM GSK2606414. After 24 h, the number of CBs was scored in n = 3 independent experiments and is shown as mean ± SD. (D) FLAG-tagged mutant ALS proteins were expressed in HeLa cells together with myc-tagged WT eIF2α or its dominant-negative S51A variant. After 24 h, cells were stained with anti-FLAG, anti-coilin and anti-myc antibodies. The CBs that were present in FLAG-positive/myc-positive cells were counted and are reported as mean ± SD from n = 3 independent experiments.

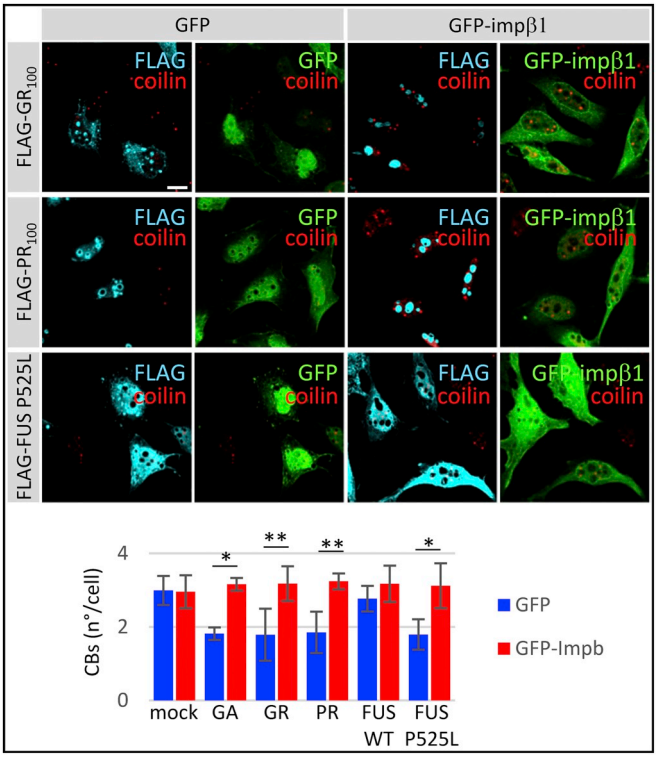

Fig. 10. Importin-β1 restores UsnRNP nuclear localization in cells expressing mutant ALS proteins. HeLa cells were transfected with plasmids coding for GFP or a GFP-tagged importin-β1, together with plasmids for the expression of FLAG-GR, FLAG-PR and FLAG-FUS P525L. After 24 h, the staining for GFP (green), FLAG (blue) and coilin (red) was collected by immunofluorescence analysis. Representative merged images are shown. Scale bar: 10 μm. The number of CBs in each condition was scored and is presented as mean ± SD from n = 3 independent experiments. $^{*}P < .05$ and $^{**}P < .01$ by t-test (GFP-Importin-β1 versus GFP-transfected cells). (For interpretation of the references to colour in this figure legend, the reader is referred to the web version of this article.)

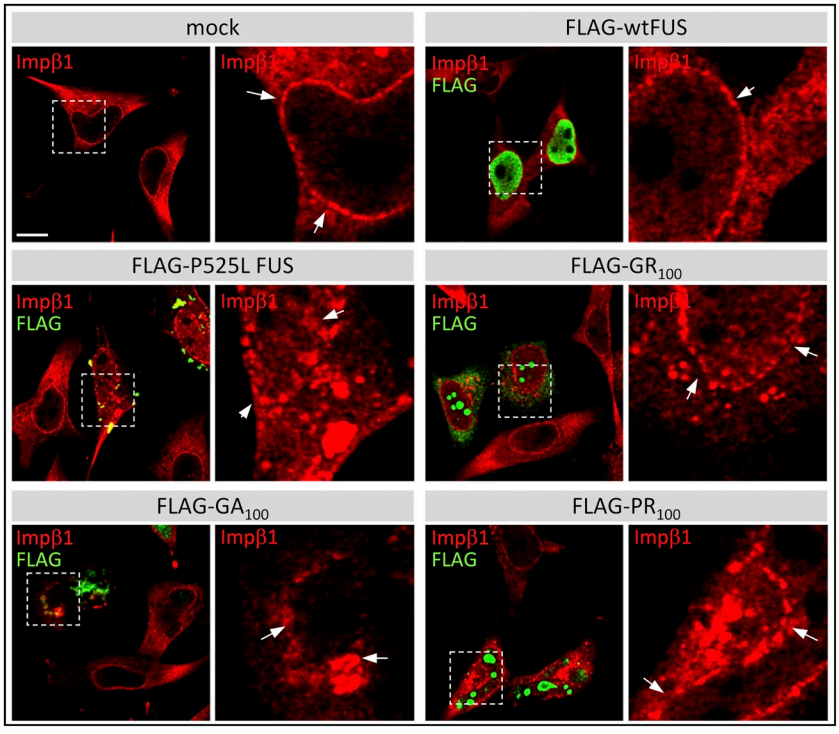

Fig. 9. Overexpression of mutant ALS proteins alters importin-β1 localization. HeLa cells were transfected with a mock plasmid or with plasmids coding for FLAG-tagged poly-GR, poly-GA, poly-PR, WT FUS and P525L mutFUS, and stained with an anti-FLAG antibody (green), and an anti-importin-β1 antibody (red). Representative magnifications of the highlighted areas are also shown. Arrows point to nuclear membrane localization of importin-β1. Scale bar: 10 μm. (For interpretation of the references to colour in this figure legend, the reader is referred to the web version of this article.)

indicate that the alteration of UsnRNP trafficking induced by mutant ALS proteins occurs downstream the ISR activation, and suggest that it might be dependent on a direct effect of mutant ALS proteins on the importin-β1-mediated trafficking of UsnRNPs. To verify this hypothesis, we therefore analysed the subcellular distribution of importin-β1 in the presence of overexpressed mutant ALS proteins. As shown in Fig. 9, importin-β1 loses its nuclear envelope localization and accumulates into cytosolic granules that occasionally co-localize with ALS protein aggregates in cells expressing DPRs or mutant FUS. Most importantly, co-expression of importin-β1 together with mutFUS or C9-DPRs rescues the number of nuclear CBs (Fig. 10), indicating that upregulating importin-β1 expression is sufficient to reverse the effects of mutant ALS proteins on their nuclear distribution.

4. Discussion

Translation inhibition is the most characterised mechanism whereby cells and organisms regulate the response to a transitory stress (Spriggs et al., 2010). Yet, the functional consequences of a chronic translation inhibition in response to persistent stress conditions are less characterised, although this condition is strongly associated to pathological states, including neurodegenerative diseases (Cestra et al., 2017; Halliday and Mallucci, 2015). Indeed, a number of proteins whose biosynthesis and localization is affected in stress conditions are required for key cellular processes, including RNA metabolism, splicing, as well as nucleo/cytosolic transport, implying that a chronic stress might have a long-term impact on these processes (Halliday et al., 2017). The most recent and straightforward example is represented by the relationship between the formation of cytoplasmic SGs that is induced by the activation of the ISR and the regulation of N/C transport of proteins and RNAs. It has been recently shown, in fact, that beyond containing RNA binding proteins as well as proteins involved in translation regulation, SGs are also populated by a number of receptors, adaptors, and other factors involved in N/C transport (Zhang et al., 2018). This finding has established the concept that regulation of N/C transport is coupled with other mechanisms that regulate stress response. However, whether the stress response modulates mRNA splicing by tuning N/C transport, is still an unanswered question. Results from our study strongly support the idea that the stress response impacts on the N/C transport of UsnRNPs, key components of the splicing machinery, thus affecting its activity. Indeed, we show here for the first time that activation of the ISR affects the localization of importin-β1 and snurportin-1, two key proteins in the nuclear import of UsnRNPs. This is associated to a significant decrease in the nuclear membrane-less granules containing assembled UsnRNPs and the SMN complex, i.e. CBs and Gems, respectively. Further, we also demonstrate that the remodelling of CBs and Gems changes alternative splicing activity. Interestingly, CB and Gem loss has been functionally related to the changes in alternative splicing regulation which occur during motor neuron degeneration in Spinal Muscular Atrophy (SMA), that is caused by the depletion of SMN, a central player in UsnRNP assembly (Cauchi, 2014). Thus, nuclear availability of UsnRNPs, that might be represented by the number of Gems and CBs, might play a crucial role in the regulation of alternative splicing. Accordingly, modifications in the splicing pattern of hnRNP A2/B1, ANKRD12 and RBM39 isoforms observed in cells treated with NaAs strongly support this conclusion. Whether the observed changes in the splicing pattern represent a defect induced by stress conditions, or rather a required modification to express specific protein isoforms involved in stress response is still unclear. Yet, it is interesting to note that the skipping of exon 8 in hnRNP A2/B1 is linked to the degeneration of motor neurons in a mouse model of familial FUS-ALS (Mirra et al., 2017), indicating that it might be associated to a pathological condition. Similarly, changes in alternative isoforms of ANKRD12 and RBM39 have been recorded in samples from C9orf72-ALS patients (Prudencio et al., 2015).

Two major pieces of evidence support the hypothesis that all these modifications are a direct consequence of changes in the N/C trafficking of UsnRNPs that are induced by ISR activation. First, inhibition of ISR by GSK2606414 or ISRIB, which act upstream or downstream of eIF2α phosphorylation, respectively, completely rescues the nuclear distribution of Gems and CBs, and restores the ratio of the splicing isoforms of hnRNP A2/B1, ANKRD12 and RBM39 to control values. Second, the overexpression of importin-β1, a key player in the nuclear import of UsnRNPs, induces a similar rescuing effect on CB and Gems distribution, suggesting that the modified localization of importin-β1 under stress is involved in the altered nuclear distribution of Gems and CBs. Interestingly, importin-β1 overexpression inhibits the formation of cytoplasmic SGs without interfering with the activation of the ISR induced by NaAs, as measured by the increased phosphorylation of eIF2α or the upregulation of ATF4 expression. This is in line with recent data showing that importin-β2, another nuclear import receptor, exerts a chaperoning role toward proteins that accumulate into SGs, promoting their dissolution (Guo et al., 2018). These observations suggest the intriguing hypothesis that a crosstalk exists between N/C transport and the ISR that orchestrates the dynamics of membrane-less organelles, such as cytoplasmic SGs and nuclear CBs/Gems, in a coordinated fashion, a conclusion reinforced by recent findings showing that the assembly of nuclear paraspeckles is intimately linked to the formation of SGs (An et al., 2019).

Most of the proteins that cause motor neuron degeneration in genetic ALS induce a significant alteration in SG dynamics, and these effects are believed to interfere with the proper localization of key factors, including RNA binding proteins, thus leading to defects in RNA metabolism (Mandrioli et al., 2019). Importantly, a wealth of data obtained from cells and animals that model genetic ALS highlighted clear defects in mRNA splicing, both in terms of the biosynthesis of the spliceosome, as well as in the regulation of alternative splicing (Gao et al., 2017). Considering the relationship between ISR activation and UsnRNP trafficking that emerged in our study, we reasoned that the splicing defects observed in ALS might be due to a reduced nuclear supply of these complexes, as a consequence of ISR-dependent defects in UsnRNP nuclear import. Indeed, our results show that the accumulation of C9orf72-derived poly-dipeptides (C9-DPRs), as well as the ALS-linked P525L mutant form of FUS, activates a widespread translational arrest and the cytosolic accumulation of SGs. Most interestingly, this correlates with a strong reduction in the number of nuclear Gems and CBs and alteration in importin-β1 localization, similarly to what observed in response to ISR activation. Unexpectedly, however, pharmacological or genetic inhibition of ISR is not sufficient to restore the nuclear distribution of Gems and CBs, while in the same experimental settings the overexpression of importin-β1 has a striking rescuing effect. These results therefore indicate that mutant ALS proteins act either independently from or just downstream ISR activation, by a direct pathological interaction with the UsnRNP import machinery. This conclusion is supported by recent results showing that both C9-DPRs and mutant FUS directly interact with UsnRNPs and that this in turn leads to alteration in the alternative splicing of target genes (Gerbino et al., 2013; Yin et al., 2017).

5. Conclusions

In conclusion, our results indicate that: i. activation of the ISR induces changes in the regulation of alternative splicing by modulating the N/C transport of UsnRNPs via the importin-β1/SPN1 import machinery, suggesting that the regulation of UsnRNP trafficking might be important for the overall regulation of gene expression in response to stress; ii. SG formation is a key event in this process, indicating that SGs act as regulators of nuclear membrane-less organelle assembly and function; iii. in ALS conditions, this regulation is impaired, and mutant ALS proteins act downstream of ISR activation by targeting the importin-β1/SPN1-mediated trafficking of UsnRNPs and affecting alternative splicing regulation.

Funding

This project was funded by Arisla (Project SPLICEALS to MC, NDA and GC), CNR Flagship Project INTEROMICS (Project PROALS to MC and GC), Ministero dell'Istruzione, Università e Ricerca (Project PRIN-2015LFPNMN to MC and NDA).

CRediT author statement

MC and SR conceived the study. SR, VR, YA, MC, SS performed the experiments; MC, SR, GC, NDA interpreted the data, prepared and wrote the manuscript. DG and AS contributed to confocal microscope analysis. MTC contributed to the experimental design. RS and CS performed experiments in primary motor neurons. MC, AS, MTC and NDA provided the financial support. All authors read and approved the final manuscript. MTC deceased on July 26th, 2018.

Declaration of Competing Interest

The authors declare that they have no competing interests.

Acknowledgments

We are grateful to Patrizia Lavia (IBPM, CNR) for kindly providing the GFP-importin-β1 plasmid, and Angelo Poletti (University of Milano) for the pCMV-DPR plasmids. We thank Francesca Di Vozzo for technical assistance.

Appendix A. Supplementary data

Supplementary data to this article can be found online at https://doi.org/10.1016/j.nbd.2020.104792.

References

An, H., et al., 2019. Stress granules regulate stress-induced paraspeckle assembly. J. Cell Biol. 218, 4127–4140.
Cauchi, R.J., 2014. Gem depletion: amyotrophic lateral sclerosis and spinal muscular atrophy crossover. CNS Neurosci. Ther. 20, 574–581.
Cestra, G., et al., 2017. Control of mRNA translation in ALS proteinopathy. Front. Mol. Neurosci. 10, 85.
Chou, C.C., et al., 2018. TDP-43 pathology disrupts nuclear pore complexes and nucleocytoplasmic transport in ALS/FTD. Nat. Neurosci. 21, 228–239.
Cristofani, R., et al., 2018. The small heat shock protein B8 (HSPB8) efficiently removes aggregating species of dipeptides produced in C9ORF72-related neurodegenerative diseases. Cell Stress Chaperones 23, 1–12.
Di Salvio, M., et al., 2015. Pur-alpha functionally interacts with FUS carrying ALS-associated mutations. Cell Death Dis. 6, e1943.
Dormann, D., et al., 2010. ALS-associated fused in sarcoma (FUS) mutations disrupt Transportin-mediated nuclear import. EMBO J. 29, 2841–2857.
Fischer, U., et al., 2011. Biogenesis of spliceosomal small nuclear ribonucleoproteins. Wiley Interdiscip. Rev. RNA. 2, 718–731.
Freibaum, B.D., Taylor, J.P., 2017. The role of dipeptide repeats in C9ORF72-related ALS-FTD. Front. Mol. Neurosci. 10, 35.
Freibaum, B.D., et al., 2015. GGGGCC repeat expansion in C9orf72 compromises nucleocytoplasmic transport. Nature. 525, 129–133.
Gao, F.B., et al., 2017. Dysregulated molecular pathways in amyotrophic lateral sclerosis-frontotemporal dementia spectrum disorder. EMBO J. 36, 2931–2950.
Gerbino, V., et al., 2013. Mislocalised FUS mutants stall spliceosomal snRNPs in the cytoplasm. Neurobiol. Dis. 55, 120–128.
Gruss, O.J., et al., 2017. UsnRNP biogenesis: mechanisms and regulation. Chromosoma. 126, 577–593.
Guo, L., et al., 2018. Nuclear-import receptors reverse aberrant phase transitions of RNA-binding proteins with prion-like domains. Cell. 173, 677–692 e20.
Halliday, M., Mallucci, G.R., 2015. Review: modulating the unfolded protein response to prevent neurodegeneration and enhance memory. Neuropathol. Appl. Neurobiol. 41, 414–427.
Halliday, M., et al., 2017. Fine-tuning PERK signaling for neuroprotection. J. Neurochem. 142, 812–826.
Kim, H.J., Taylor, J.P., 2017. Lost in transportation: nucleocytoplasmic transport defects in ALS and other neurodegenerative diseases. Neuron. 96, 285–297.
Lott, K., Cingolani, G., 2011. The importin beta binding domain as a master regulator of nucleocytoplasmic transport. Biochim. Biophys. Acta 1813, 1578–1592.
Mandrioli, J., et al., 2019. ALS and FTD: where RNA metabolism meets protein quality control. Semin. Cell Dev. Biol. https://doi.org/10.1016/j.semcdb.2019.06.003. pii: S1084-9521(18)30200-3.
Matera, A.G., Wang, Z., 2014. A day in the life of the spliceosome. Nat. Rev. Mol. Cell Biol. 15, 108–121.
Medelin, M., et al., 2018. Exploiting natural polysaccharides to enhance in vitro bioconstructs of primary neurons and progenitor cells. Acta Biomater. 73, 285–301.
Mirra, A., et al., 2017. Functional interaction between FUS and SMN underlies SMA-like splicing changes in wild-type hFUS mice. Sci. Rep. 7, 2033.
Narayanan, U., et al., 2002. SMN, the spinal muscular atrophy protein, forms a pre-import snRNP complex with snurportin1 and importin beta. Hum. Mol. Genet. 11, 1785–1795.
Nussbacher, J.K., et al., 2019. Disruption of RNA metabolism in neurological diseases and emerging therapeutic interventions. Neuron. 102, 294–320.
Prudencio, M., et al., 2015. Distinct brain transcriptome profiles in C9orf72-associated and sporadic ALS. Nat. Neurosci. 18, 1175–1182.
Rabouw, H.H., et al., 2019. Small molecule ISRIB suppresses the integrated stress response within a defined window of activation. Proc. Natl. Acad. Sci. U. S. A. 116, 2097–2102.
Reber, S., et al., 2016. Minor intron splicing is regulated by FUS and affected by ALS-associated FUS mutants. EMBO J. 35, 1504–1521.
Rossi, S., et al., 2015. Nuclear accumulation of mRNAs underlies G4C2-repeat-induced translational repression in a cellular model of C9orf72 ALS. J. Cell Sci. 128, 1787–1799.
Scardigli, R., et al., 2001. Crossregulation between Neurogenin2 and pathways specifying neuronal identity in the spinal cord. Neuron. 31, 203–217.
Scardigli, R., et al., 2014. Neutralization of nerve growth factor impairs proliferation and differentiation of adult neural progenitors in the subventricular zone. Stem Cells 32, 2516–2528.
Sidrauski, C., et al., 2015. The small molecule ISRIB reverses the effects of eIF2alpha phosphorylation on translation and stress granule assembly. Elife. 4 e05033.
Spriggs, K.A., et al., 2010. Translational regulation of gene expression during conditions of cell stress. Mol. Cell 40, 228–237.
Steyaert, J., et al., 2018. FUS-induced neurotoxicity in Drosophila is prevented by downregulating nucleocytoplasmic transport proteins. Hum. Mol. Genet. 27, 4103–4116.
Woerner, A.C., et al., 2016. Cytoplasmic protein aggregates interfere with nucleocytoplasmic transport of protein and RNA. Science. 351, 173–176.
Yin, S., et al., 2017. Evidence that C9ORF72 dipeptide repeat proteins associate with U2 snRNP to cause Mis-splicing in ALS/FTD patients. Cell Rep. 19, 2244–2256.
Yu, Y., et al., 2015. U1 snRNP is mislocalized in ALS patient fibroblasts bearing NLS mutations in FUS and is required for motor neuron outgrowth in zebrafish. Nucleic Acids Res. 43, 3208–3218.
Zhang, K., et al., 2018. Stress granule assembly disrupts nucleocytoplasmic transport. Cell 173, 958–971 e17.